Progress In Electromagnetics Research, PIER 93, 291–306, 2009

VECTOR HOPKINS MODEL RESEARCH BASED ON OFF-AXIS ILLUMINATION IN NANOSCALE LITHOGRAPHY

P. F. Cao, L. Cheng, and X. P. Zhang

School of Information Science and Engineering
Lanzhou University
Lanzhou 730000, China

Abstract—Based on vector electromagnetic theory and the Waveguide Model, the vector Hopkins model is deduced. The model contains the vector Hopkins formula and the resist profile model of fast Optical Proximity Correction. The vector Hopkins formula considers incidence angles and azimuth angles of off-axis illumination, which differs from the traditional scalar Hopkins formula. The resist profile model is employed to analyze the effect of the photoresist diffusion under off-axis illumination by using self-adaptive Gaussian filter with scale adjustable, and a new transmission cross coefficient is obtained. The projection system parameters are introduced simultaneously, such as incidence angles, azimuth angles of off-axis illumination and diffusion parameters of photoresist. By simulating the aerial image of 3D mask in the actual lithography process, the optimal angular range of oblique incidence is studied; the image quality by impact with the oblique incidence angle is discussed as well.

1. INTRODUCTION

The steadily decreasing dimensions in semiconductor devices are for filling the requirement of the increased resolution in nanolithography. Off-axis illumination (OAI) as one of the important resolution enhancement techniques is applied to achieve the higher resolution [1]. However, the models like Optical Proximity Correction (OPC) which utilize the OAI are still using the thin film mask approximation method (Kirchhoff approach or scalar Hopkins model). In this Kirchhoff approach framework where the mask is considered as an infinitely thin film, the diffracted orders of an oblique incident light under the

Corresponding author: X. P. Zhang (zxp@lzu.edu.cn).

condition of OAI are assimilated as the normal incident waves and calculated by a simple shift in the Fourier spectrum. This is only valid in Kirchhoff approach where the near-field calculation of the diffractions at mask edges is not included. Recent research results have demonstrated the limitations of Kirchhoff approach in the paper of OAI concerned [2, 3]. Vector lithography simulation has been becoming more and more important. Three-dimensional (3D) simulation is necessary for accurate modeling in such critical problems, e.g., 3D defects, 3D mask repair and optical proximity effects. However, the major disadvantage of 3D rigorous vector simulation is the huge increased computation time and memory requirements over 3D scalar models and 2D vector models [4, 5]. Based on this, and taking the OPC model into account, computation load is much heavier. The final aim of OPC model is to reduce the amount of calculation and improve accuracy at the same time. However, the traditional resist profile model of fast OPC, which was used to simulate the photoresist diffusion, usually can be simulated by a Transmission Cross Coefficient (TCC) convoluting a simple 2D Gaussian filter [6] and ignored effects caused by the scale parameter σ of Gaussian filter, so it was not accuracy enough for 3D mask in OAI.

In this paper, a new vector Hopkins model is proposed to improve operational precision in nanolithography simulation. The model contains the vector Hopkins formula and the modified resist profile model of fast OPC. The vector Hopkins formula is deduced by using Vector Electromagnetic Theory [7–11] and Waveguide Models [12]. The new formula contains the incidence angles and the azimuth angles of off-axis illumination, which is different from the traditional scalar Hopkins formula. Based on this vector formula, the modified resist profile model of fast OPC is obtained by convolving self-adaptive Gaussian filter with scale adjustable, which is proposed firstly in this manuscript, and a new transmission cross coefficient ($\widetilde{TCC}$) is obtained as well. The $\widetilde{TCC}$ includes the projection system parameters such as incidence angles, azimuth angles of off-axis illumination and photoresist diffusion of parameters. The image quality depending on the incidence angles is investigated and the best range of illumination is concluded. These results are verified by our simulations compared with scalar Hopkins formula. Finally the run time and required memory by using the vector Hopkins model are compared with the rigorous vector simulation method, and the result indicates that the vector Hopkins model is a fast and precise simulation method.

2. THEORY

2.1. Vector Hopkins Formula

In order to calculate the 3D mask accurately, the additional parameters including incidence angles and incidence azimuth angles of the illumination source are taken into account to descript the OAI model in this paper as shown in Figure 1.

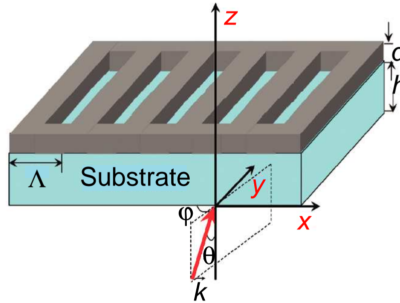

Figure 1. Incidence light and 3D mask schematics.

In Figure 1, Λ is the period along the X-axis direction of mask pitch, $\vec{K}$ is the incident wave vector, θ is the incident angle which is the intersection angle between the incident wave vector and Z-axis, and φ is the incident azimuth angle which is the intersection angle between projection vector of $\vec{K}$ in X-Y plane and X-axis. And we assume that the evanescent waves are not contained in the incident field.

The j-order diffraction vector electric field can be calculated by applying the Rigorous Diffraction Theory and the electromagnetic field boundary conditions [7]:

$$\vec{E}_j = \vec{A}_j \exp\left\{-i\left[\vec{k}_{xj}x + \vec{k}_y y + \vec{k}_{zj}z\right]\right\} \tag{1}$$

where j is an integer referring to a diffraction order, $\vec{A}_j$ is the vector transmission amplitude, $k_{xj} = K_x + \frac{2\pi}{\Lambda}j$, $K_x = \frac{2\pi}{\lambda}\sin\theta\cos\phi$, $k_y = \frac{2\pi}{\lambda}\sin\theta\sin\phi$ and $k_{zj} = \sqrt{\left(\frac{2\pi}{\lambda}n\right)^2 - k_y^2 - k_{xj}^2}$ are the components of wave vector along the X-axis, Y-axis and Z-axis, respectively. The j-order diffraction vector magnetic field has the similar form which corresponds with the vector electric field.

Applying the electromagnetic field diffraction operation [7, 13], one obtains the following expressions for the fields which incident

on the Entrance Pupil (EP) in the Fresnel region of the diffracted field [14, 15]:

Applying the electromagnetic field diffraction operation [14], one obtains the following expressions for the fields which incident on the Entrance Pupil (EP) in the Fresnel region of the diffracted field [15]:

$$\vec{E}_{EPj}\left(K_x, K_y; k_{xj}, k_y\right) = \frac{j}{4\pi}\frac{e^{jR}}{R}\mathbf{F}\left\{\left[\sqrt{\frac{\mu_0}{\varepsilon_0}}\left(\vec{z}\times\vec{H}_j\right)-\left(\vec{z}\times\vec{E}_j\right)\times\vec{K} - \left(\vec{z}\cdot\vec{E}_j\right)\vec{K}\right]; \frac{k_{xj}}{\lambda}, \frac{k_y}{\lambda}\right\} \tag{2}$$

$$\vec{H}_{EPj}\left(K_x, K_y; k_{xj}, k_y\right) = -\frac{j}{4\pi}\frac{e^{jR}}{R}\mathbf{F}\left\{\left[\sqrt{\frac{\varepsilon_0}{\mu_0}}\left(\vec{z}\times\vec{E}_j\right)+\left(\vec{z}\times\vec{H}_j\right)\times\vec{K} + \left(\vec{z}\cdot\vec{H}_j\right)\vec{K}\right]; \frac{k_{xj}}{\lambda}, \frac{k_y}{\lambda}\right\} \tag{3}$$

where $\mathbf{F}$ denotes Fourier Transformation, R is the distance from the intersection point O of the mask with the optical axis to an observation point Q on the EP.

The electric vector $\vec{E}_{EPj}$ at a point on EP is rotated into electric vector $\vec{E}_{XPj}$ at the corresponding point on the Exit Pupil (XP) [16].

$$\vec{E}_{XPj}\left(K_x,\, K_y;\, s_{xj},\, s_y\right) = \mathbf{M}\left(s_{xj},\, s_y\right)\times\vec{E}_{EPj}\left(K_x,\, K_y;\, s_{xj},\, s_y\right) \tag{4}$$

where $(s_{xj},\, s_y) = (k_{xj}/m,\, k_y/m)$, m represents the magnification, and $\mathbf{M}$ represents the lens matrix.

$$\mathbf{M}\left(s_{xj},\, s_y\right) = \begin{bmatrix} s_y^2 & -s_{xj}s_y & 0 \\ -s_{xj}s_y & s_{xj}^2 & 0 \\ (K_x s_{xj}+K_y s_y)s_{xj}s_z & (K_x s_{xj}+K_y s_y)s_y s_z & (K_x s_{xj}+K_y s_y)(s_{xj}^2+s_y^2) \end{bmatrix} \tag{5}$$

Hence the vector electric field on the optics image can be represented [17, 18]:

$$\vec{E} = \iint_{\sqrt{s_{xj}^2+s_y^2}\le NA} \vec{A}\left(s_{xj},\, s_y\right)\times e^{i(s_{xj}x+s_y y+s_z z)}ds_{xj}ds_y \tag{6}$$

where $(s_{xj},\, s_y,\, s_z)$ represents the direction of propagation parameter, and $\vec{A}$ is the amplitude vector:

$$\vec{A}\left(s_{xj},\, s_y;\, K_x,\, K_y\right) = \frac{m}{j\lambda^2}\sqrt{\frac{\vec{z}\cdot\vec{k}}{\vec{z}\cdot\vec{K}}}\mathbf{M}\left(s_{xj}, s_y\right)\mathbf{F}\left\{\vec{E}_j; \frac{s_{xj}-K_x}{\lambda}, \frac{s_y-K_y}{\lambda}\right\} \times e^{i[\Phi(s_{xj}, s_y)-s_{xj}\Delta]} \tag{7}$$

where $\Phi(s_{xj}, s_y)$ is the aberration function, and Δ is the defocus distance.

Next, the intensity distributions on the wafer. We assume that the wafer grating structure is invariant along the $\pm\vec{y}$ directions, and the structure with nonvertical sidewalls is approximated by stratifying it into many thin sublayers with vertical sidewalls. The traveling direction of the incident wave E is restricted to be on the xz plane and thus the scattered waves are also on the same plane symmetrically. Then the amplitude on the wafer could be computed using the waveguide model [12].

In order to increase the speed of calculation, the incident electromagnetic wave is divided into TE polarization and TM polarization and then the components are studied respectively.

2.1.1. TE Mode

Inside a stratified layer i, the electric and magnetic fields are expressed by

$$E_y^i = \sum_{m=-L}^{L}\left[\left(F_m^i e^{\alpha_m^i(z-z_{i-1})} + F_m'^i e^{-\alpha_m^i(z-z_{i-1})}\right)\times\sum_{l=-L}^{L} G_{lm}^i e^{il(s_{xj}x+s_y y)}\right] \tag{8}$$

$$H_x^i = -\sum_{m=-L}^{L}\left[\left(F_m^i e^{\alpha_m^i(z-z_{i-1})} - F_m'^i e^{-\alpha_m^i(z-z_{i-1})}\right)\times\sum_{l=-L}^{L} G_{lm}^i e^{il(s_{xj}x+s_y y)}\right] \tag{9}$$

where L is proportional to the number of traveling waves in the calculation.

By using the Waveguide Model in [12], the electric field in Y direction is deduced:

$$\begin{aligned} E_y &= \sum_{i=-0}^{N}\left(\sum_{m=-L}^{L}\left[\left(F_m^i e^{\alpha_m^i(z-z_{i-1})} + F_m'^i e^{-\alpha_m^i(z-z_{i-1})}\right)\right.\right. \\ &\qquad \left.\left.\times\sum_{l=-L}^{L} G_{lm}^i e^{il(s_{xj}x+s_y y)}\right]\right) = E_y^{(+)} + E_y^{(-)} \end{aligned} \tag{10}$$

where $E_y^{(+)}$ and $E_y^{(-)}$ are the electric components of downgoing (+) and upgoing (−) waves, respectively, at the depth of z in the photoresist correlated with the incident electric wave in TE-polarization.

2.1.2. TM Mode

Following the Section 2.1.1, we obtain the magnetic field in Y direction, which is described as:

$$H_y = \sum_{i=0}^{N}\left(-\sum_{m=-L}^{L}\left[\left(F_m^i e^{\alpha_m^i(z-z_{i-1})} - F_m'^i e^{-\alpha_m^i(z-z_{i-1})}\right) \times \sum_{l=-L}^{L} G_{lm}^i e^{il(s_{xj}x+s_y y)}\right]\right) = H_y^{(+)} + H_y^{(-)} \quad (11)$$

where $H_y^{(+)}$ and $H_y^{(-)}$ are the magnetic components of the downgoing (+) and upgoing (−) waves, respectively, at the depth of z in the photoresist due to incident magnetic wave in TM-polarization.

2.1.3. Common Conditions

The incident electromagnetic waves can be generally described by non-coherently superposing TE model and TM mode. As introduced in the Section 2.1.1 and Section 2.1.2, the final amplitude vector of the incident wave on the wafer is shown as below:

$$\vec{B}(s_{xj}, s_y) = \left[\vec{A}(s_{xj}, s_y)\cdot\vec{e}_\perp\right]\left[E_y^{(+)} + E_y^{(-)}\right]\vec{e}_\perp + \left[\vec{A}(s_{xj}, s_y)\cdot\vec{e}_{//}\right]\frac{1}{n_r}\left[H_y^{(+)}\left(\vec{e}_\perp \times \vec{s}_r^{(+)}\right) + H_y^{(-)}\left(\vec{e}_\perp \times \vec{s}_r^{(-)}\right)\right] \quad (12)$$

where the first item denotes TE-polarization and the second one denotes TM-polarization. Besides, n_r is the complex refractive index of photoresist and $\overrightarrow{s_r^{(\pm)}}$ is the propagation vectors of the downgoing (+) and upgoing (−) waves, respectively. In the photoresist, the unit vectors $\vec{e}_\perp = \frac{\vec{z}\times\vec{K}}{\left|\vec{z}\times\vec{K}\right|}$ and $\vec{e}_{//} = \vec{e}_\perp \times \vec{K}$ are normal direction and tangential direction, respectively. ($\vec{s}$ is the unit vector of $\vec{A}$). Based on (5) and (7), $A(s_{xj}, s_y)$ can be written in a matrix form. It is substituted back in (12), we obtain

$$\mathbf{B}(s_{xj}, s_y) = \mathbf{P}_{ij}(s_{xj}, s_y)\mathbf{A}(s_{xj}, s_y), \qquad i, j = 1, 2, 3 \quad (13)$$

when (11) is substituted back in (18), we obtain

$$\mathbf{B}(s_{xj}, s_y; K_x, K_y) = \frac{m}{i\lambda^2}\mathbf{K}_{ij}\left(\frac{s_{xj}}{\lambda}, \frac{s_y}{\lambda}; z\right) \times \mathbf{F}\left\{E_j; \frac{s_{xj}-K_x}{\lambda}, \frac{s_y-K_y}{\lambda}\right\} \quad (14)$$

in which

$$\mathbf{K}_{ij} = \sqrt{\frac{\vec{z}\cdot\vec{r}}{\vec{z}\cdot\vec{s}}}\,\mathbf{P}_{ij}(s_{xj},\, s_y)\mathbf{M}(s_{xj},\, s_y)e^{i[\Phi(s_{xj},\, s_y)-s_{xj}\Delta]}. \tag{15}$$

2.1.4. Intensity Computation

Applying Abbe Principle and the intensity definition [3], the final intensity can be obtained:

$$\begin{aligned} I(x,\, y,\, z) \;=\; & \iint J(K_x,\, K_y)\left| \iint \mathbf{B}(s_{xj},\, s_y;\, K_x,\, K_y) \right. \\ & \left. \times e^{i(s_{xj}x+s_y y)} ds_{xj} ds_y \right|^2 dK_x dK_y \end{aligned} \tag{16}$$

where $J(K_x,\, K_y)$ is the intensity of the source.

When (14) is substituted back in (16), we obtain the vector Hopkins formula:

$$\begin{aligned} I(x,\, y,\, z) \;=\; & \iiiint ds_{xj} ds_y ds'_{xj} ds'_y \iint J(K_x,\, K_y) \\ & \times \mathbf{K}_{ik}\left(\frac{s_{xj}}{\lambda},\, \frac{s_y}{\lambda};\, z\right)\mathbf{K}^*_{kj}\left(\frac{s'_{xj}}{\lambda},\, \frac{s'_y}{\lambda};\, z\right) \\ & \times e^{i[(s_{xj}-s'_{xj})x+(s_y-s'_y)y]}\frac{m^2}{\lambda^4}\times \mathbf{F}\left\{E_j;\, \frac{s_{xj}-K_x}{\lambda},\, \frac{s_y-K_y}{\lambda}\right\} \\ & \times \mathbf{F}^*\left\{E_j;\, \frac{s'_{xj}-K_x}{\lambda},\, \frac{s'_y-K_y}{\lambda}\right\} dK_x dK_y \\ =\; & \iiiint T_{ij}\mathbf{F}\left\{E_j;\, \frac{s_{xj}-K_x}{\lambda},\, \frac{s_y-K_y}{\lambda}\right\} \\ & \quad \times \mathbf{F}^*\left\{E_j;\, \frac{s'_{xj}-K_x}{\lambda},\, \frac{s'_y-K_y}{\lambda}\right\} \\ & \quad \times e^{i[(s_{xj}-s'_{jx})x+(s_y-s'_y)y]} ds_{xj} ds_y ds'_{xj} ds'_y \end{aligned} \tag{17}$$

where the Transmission Cross Coefficient (TCC) is

$$T_{ij} = \iint J(K_x,\, K_y)\mathbf{K}_{ik}\left(\frac{s_{xj}}{\lambda},\, \frac{s_y}{\lambda};\, z\right)\mathbf{K}^*_{kj}\left(\frac{s'_{xj}}{\lambda},\, \frac{s'_y}{\lambda};\, z\right) dK_x dK_y \tag{18}$$

(s'_{xj}, s'_y) is the conjugate component of (s_{xj}, s_y). Since (18) contains the incidence angles and azimuth angles of OAI, it is so-called vector TCC.

The vector Hopkins formula of (17) is identical with the scalar Hopkins formula [3] in form. When $\theta = 0$ and $\varphi = 0$, (17) can be reverted into the scalar Hopkins formula.

2.2. The Resist Profile Model

The photoresist diffusion model is used to characterize the accurate resist profile simulation for OPC. In [6], according to adjust the only parameter of Gaussian filter — standard deviation, the effect of the photoresist diffusion can be simulated by TCC convoluting a simple 2D Gaussian filter. However, this method considers neither the influence of incidence angles under OAI nor the filter effect for Gaussian filter. Practically, the Gaussian filter usage in image processing is that the scale parameter σ of Gaussian filter is required as larger as possible corresponding to the image edge, and while σ is required as smaller as possible corresponding to the image smoothing department. Evidently, how to choose the optimum value of σ is important to the resist profile simulation. So, self-adaptive Gaussian filter with scale adjustable is designed.

2.2.1. Self-adaptive Gaussian Filter with Scale Adjustable Model

Two-dimensional (2D) Gaussian filter is

$$G(x, y) = \frac{1}{2\pi\sigma^2} e^{\left(-\frac{x^2+y^2}{2\sigma^2}\right)} \tag{19}$$

As TN Cornsweet [19] has used the image pixel grayscale value countdown as the pixel related to σ, the problem of choosing σ can be transformed to the judgment of the current image pixel of the region smoothness problem.

We assume the current image pixel is (x, y), the filter window is $m \times n$, the image signal is $L(x, y)$, and the sampling image signal of the filter window is $L_{(i,j)}(x, y)$, so the average grayscale value of corresponding image window is

$$M_w(x, y) = \frac{1}{m \times n} \sum_{i=-(m+1)/2}^{(m+1)/2} \sum_{j=-(n+1)/2}^{(n+1)/2} L_{(i,j)}(x, y) \tag{20}$$

The difference of the current pixel's grayscale value and the average grayscale value of corresponding image window is

$$D(x, y) = |L(x, y) - M_w(x, y)| \tag{21}$$

Because $M_w(x, y)$ represents the smoothness of image window, $D(x, y)$ is inversely proportioned to the smoothness of image window.

So the Gaussian filter standard deviation is

$$\sigma = D(x, y) = |L(x, y) - M_w(x, y)| = \left| L(x, y) - \frac{1}{mn} \sum_{i=-(m+1)/2}^{(m+1)/2} \sum_{j=-(n+1)/2}^{(n+1)/2} L_{(i,j)}(x, y) \right| \quad (22)$$

When (22) is substituted back in (19), the self-adaptive Gaussian Filter with scale adjustable is obtained.

2.2.2. The Resist Profile Model

Then the self-adaptive Gaussian Filter with scale adjustable convolutes (17), we obtain the simplification expression:

$$\begin{aligned} I_{eff}(x, y) &= I(x, y) * G(x, y) \\ &= \int_{-\infty}^{\infty}\int_{-\infty}^{\infty} \left(\iiiint TCC_{ij} \times G(x-u, y-v) \times \mathbf{F} \right. \\ &\quad \left. \times \mathbf{F}^* \times e^{i[(s_{xj}-s'_{jx})x+(s_y-s'_y)y]} ds_{xj} ds_y ds'_{xj} ds'_y \right) dudv \\ &= \iiiint \widetilde{TCC} \times \mathbf{F} \times \mathbf{F}^* \times e^{i[(s_{xj}-s'_{jx})x+(s_y-s'_y)y]} ds_{xj} ds_y ds'_{xj} ds'_y \quad (23) \end{aligned}$$

in which

$$\widetilde{TCC} = \int_{-\infty}^{\infty}\int_{-\infty}^{\infty} TCC_{ij} \times G(x-u, y-v)\, dudv \quad (24)$$

(24) is so-called $\widetilde{TCC}$. It contains the projection system parameters such as incidence angles, azimuth angles of off-axis illumination and diffusion of photoresist of parameters.

2.3. The Matrix Decomposition Algorithm of $\widetilde{TCC}$

Since the $\widetilde{TCC}$ includes various parameters of the projection system, the algorithm of $\widetilde{TCC}$ becomes particularly important. When the dielectric constant of wafer is real, the $\widetilde{TCC}$ function is a complex Hermitian matrix, and the decomposition on $\widetilde{TCC}$ can be transformed to solve Hermitian matrix eigenvalues problem. Weilandt-Hoffman theorem has proved that eigenvalues of Hermitian matrix are not

sensitive to small perturbations of the matrix elements [20]. So the Hermitian matrix can be directly transformed into a symmetric diagonal matrix. There are many algorithms to solving eigenvalues of the symmetric diagonal matrix, and we use the RRR (Relative Robust Representation) algorithm, which is considered to use the smallest work space [21]. When the dielectric constant of wafer is not real, the $\widetilde{TCC}$ function is a general matrix, and the eigenvalues and eigenvectors of $\widetilde{TCC}$ can be obtained by numerical methods, whose computation load is big. The genetic algorithm [22] can raise the computation speed, and our algorithm in this paper comes from [23].

3. SIMULATION RESULTS

MATLAB is used to simulations. Firstly, diffraction intensity distributions of the single slit mask are computed by (22). The width of the slit is 155 nm. Assumed the incidence wavelength is 193 nm, and the electromagnetic wave is incident through the mask with different incidence angles. The results are as shown in Figures 2–5.

In Figure 2, the 1-order diffraction intensity distributions for different incidence angles are compared, in which azimuth angles are invariable. Figure 2 shows the central place of intensity shifts with the incident angle, the intensity amplitude and the lobe width are also changed when the incident angle changed. But the decrease of the intensity amplitude is more obvious for 85 degree incidence angle in Figure 2, where OPE is quite prominent. Relatively, the peak value

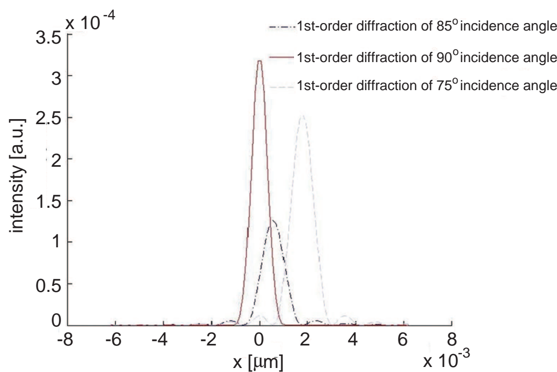

Figure 2. 1st-order diffraction intensity distributions within incidence angles.

in 75 degree incidence angle is approaching the max. The 0-order diffraction situation is similar to 1-order diffraction.

In Figure 3, the azimuth angles with corresponding incidence angles by (22) are compared. It shows that the incident azimuth only influences the intensity amplitude.The results of the periodic mask are similar, so we do not repeat that for the paper length limit.

Because the position of reflective spot was measured to detect the silicon chip platform's horizontal position in the circumstance of industry, we can acquire the reflectivity of the light reflected by

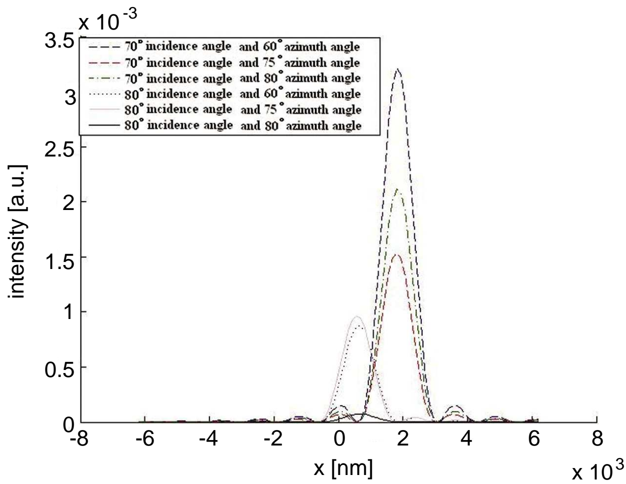

Figure 3. The diffraction intensity distributions within the incident azimuth.

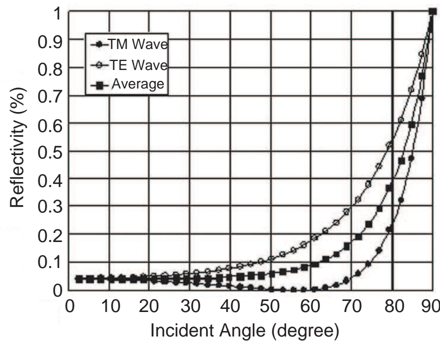

Figure 4. Index of reflection and the incidence angle.

the topside of the mask and determine the best oblique illumination incidence angle. And the reflectivity formula is

$$\Gamma = \frac{I_{inc} - I}{I_{inc}} \tag{25}$$

where I_{inc} is the normalization intensity, I is the intensity thru the mask. (17) is normalized and substituted back in (25), the relational curve is obtained as shown in Figure 4. It shows the lowest reflectivity is between 60–75 degrees in the large numerical aperture, and the luminous intensity transmissibility is quite high.

Furthermore, the photoresist profile is simulated by using a simple 2D Gaussian filter and (23), respectively, as shown in Figures 5(a) and 5(b). It shows that the effect of photoresist diffusion in wafer profile can be accurately simulated by using our Gaussian model.

To further confirm the vector Hopkins formula inferred in this paper, a simple diplo-hole mask is simulated, as shown in Figure 6. The simulation image by using the scalar, vector Hopkins formula and rigorous coupled-wave analysis (RCWA) [24–26] are shown in Figures 6(b), (c) and (d), respectively. By contrasting (b) with (c),

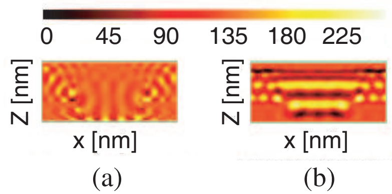

Figure 5. Simulation result on resist profile. (a) The resist profile by using the simple 2D Gaussian filter model. (b) The resist profile by using the adaptive Gaussian filter with scale adjustable model.

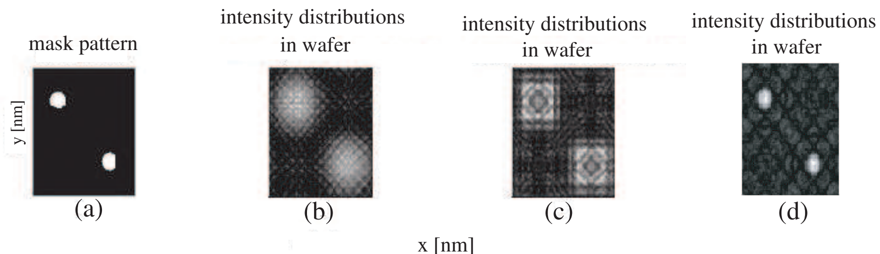

Figure 6. Simulation result on wafer: (a) a mask pattern; (b) the scalar Hopkins formula; (c) the vector Hopkins formula; (d) the rigorous coupled-wave analysis

the image pattern with vector Hopkins formula simulation is much distinct. By contrasting (d) with (c), the image pattern error is not obvious. Figure 7 shows the 3D intensity distributions of the mask pattern is simulated by scalar, vector Hopkins formula and RCWA, and results are shown in Figures 7(a), (b) and (c), respectively. We find that the diffraction intensity is most centralized by using RCWA, next is using the vector Hopkins formula. The comparative results between our model and scalar Hopkins method correspond with the comparative results between the rigorous vector simulation method and scalar Hopkins method [24].

Finally, the computation time, the memory requirements and amplitude error of intensity by using the vector Hopkins method are compared with the RCWA. Taking a 70 degrees oblique TE wave illuminates aforementioned single slit mask as an example, the 1st-

Table 1. Run time and memory comparison of the vector Hopkins method and RCWA.

Method	Vector Hopkins Method	RCWA
Run time	128.046000 seconds	177.2800000 seconds
Memory required	102 Meg	119 Meg

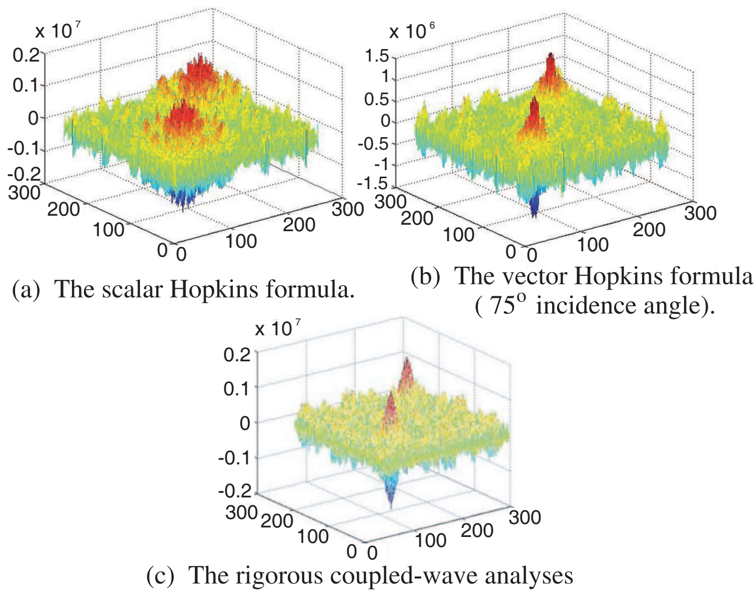

(a) The scalar Hopkins formula.

(b) The vector Hopkins formula (75° incidence angle).

(c) The rigorous coupled-wave analyses

Figure 7. 3D-intensity distributions.

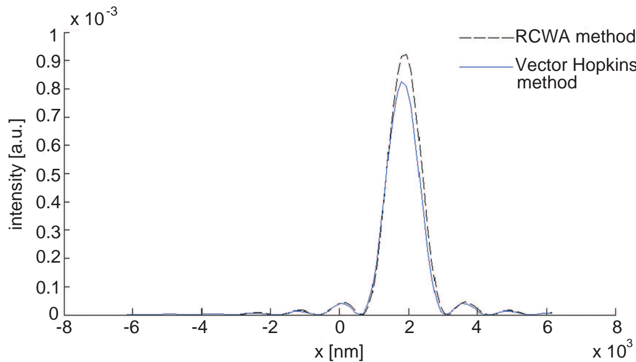

Figure 8. 1st-order diffraction intensity distributions of vector Hopkins method and RCWA.

order diffraction intensity distributions is calculated, as shown in Figure 8, and the results of this comparison are shown in Table 1. Obviously, computation time and the memory requirements are reduced by using the vector Hopkins method. The reason is that this method is not necessary to incorporate many evanescent waves into simulations because of the strong filtering by the projection lens. As shown in Figure 8, there is tiny amplitude error of intensity, which is less than 10^{-4}. So, the vector Hopkins model is a fast and precise model.

4. CONCLUSION

The vector Hopkins formula is deduced in our work. It contained the projection system parameters such as incidence angles, azimuth angles and photoresist diffusion of parameters. It is observed that the lithography imaging depends on the incidence angles and azimuth angles. The best oblique incidence angle scope to OAI lithography is investigated. Meanwhile, the new transmission cross coefficient ($\widetilde{TCC}$) is used for fast precise simulation. The evaluation shows that the vector Hopkins formula provides improved accuracy compared with scalar Hopkins formula under hyper NA and Off-axis Illumination lithography simulation. And the computation time the memory requirements are smaller by using vector Hopkins model. Therefore the model has well serviceability and application prospect.

REFERENCES

1. Inazuki, Y. C., "Analysis of diffraction orders including mask topography effects for OPC optimization," *Proc. of SPIE on*

Optical Microlithography XX, Vol. 6520, 65204S, San Jose, CA, USA, 2007.

2. Pistor, T. V., A. R. Neureuther, and R. J. Socha, "Modeling oblique incidence effects in phoromasks," *Proc. of SPIE on Optical Microlithography XIII*, Vol. 4000, 228, Santa Clara, CA, USA, 2000.
3. Born, M. and E. Wolf, *Principles of Optics*, Pergamon Press, 1980.
4. Saied, M., F. Foussadier, and J. Belledent, "3D mask modeling with oblique incidence and mask corner rounding effects for the 32 nm mode," *Proc. of SPIE on Photomask Technology*, Vol. 6730, Monterey, CA, USA, 2007.
5. Liu, P., Y. Cao, and L. Chen, "Fast and accurate 3D mask model for full-chip OPC and verification," *Proc. of SPIE on Optical Microlithography XX*, Vol. 6520, San Jose, CA, USA, 2007.
6. Inui, H. and T. Ohta, "A practical 3D lithography simulation system," *SPIE*, Vol. 3051, 522–528, 1997.
7. Stratton, J., *Electromagnetic Theory*, McGraw-Hill Book Company, 1941.
8. Guo, L., Y. Wang, R. Wang, and Z.-S. Wu, "Investigation on the electromagnetic scattering of plane wave/Gaussian beam by adjacent multi-particles," *Progress In Electromagnetics Research B*, Vol. 14, 219–245, 2009.
9. Giampaolo, Di, E. and F. Bardati,, "A projective approach to electromagnetic propagation in complex environments," *Progress In Electromagnetics Research B*, Vol. 13, 357, 2009.
10. Ayub, M., A. B. Mann, M. Ramzan, and M. H. Tiwana, "Diffraction of plane waves by a slit in an infinite soft-hard plane," *Progress In Electromagnetics Research B*, Vol. 11, 103–131, 2009.
11. Molinet, F. A., "Plane wave diffraction by a strongly elongated object illuminated in the paraxial diretion," *Progress In Electromagnetics Research B*, Vol. 6, 135–151, 2008.
12. Yuan, C. M., "Efficient light scattering modeling for alignment, metrology, and resist exposure in photolithography," *J. Opt. Soc. Amer.*, Vol. 8, 778, 1991.
13. Rahim, T., M. J. Mughal, Q. A. Naqvi, and M. Faryad, "Field around the focal region of a paraboloidal reflector placed in isotropic chiral medium," *Progress In Electromagnetics Research B*, Vol. 15, 57–76, 2009.
14. Yeung, M. S. and D. Lee, "Extension of the Hopkins theory of partially coherent imaging to include thin-film interference effects," *Proc. of SPIE on Optical/Laser Microlithography*,

Vol. 1927, 452–463, San Jose, CA, USA, 1993.

15. McCartin, B. J., L. J. Bahrmasel, and G. Meltz, "Application of the control region approximation to two-dimensional electromagnetic scattering," *Progress In Electromagnetics Research*, PIER 02, 175–21, 1990.
16. Yeung, M. S., "Modelling high numerical aperture optical lithography," *Proc. SPIE*, Vol. 922, 149–167, 1988.
17. Wolf, E., "Electromagnetic diffraction in optical system I. An integral representation of the image field," *Proc. Roc. Soc. A*, Vol. 253, 349–357, 1959.
18. Hatamzadeh-Varmazyar, S. and M. Naser-Moghadasi, "An integral equation modeling of electromagnetic scattering from the surfaces of arbitrary resistance distribution," *Progress In Electromagnetics Research B*, Vol. 3, 157–172, 2008.
19. Cornsweet, T. N. and J. I. Yellott, "Intensity dependent spatial summation," *Journal of Optical Society of America A*, Vol. 2, No. 10, 1769–1786, 1985.
20. Golub, G. H. and C. F. Van Loan, *Matrix Computations*, JHU Press, 1996.
21. Dhillon, I., "A new $O(n^2)$ algorithm for the symmetric tri-diagonal eigenvalue/eigenvector problem," University of California Report, Berkeley, 1997.
22. Holland, J. H., *Adaptation in Nature and Artificial Systems*, The University of Michigan Press, 1975.
23. Raymer, M. L. and W. F. Punch, "Dimensionality reduction using genetic algorithms," *IEEE Transactions on Evolutionary Computation*, Vol. 4, 164–171, 2000.
24. Bruge, S., "Rigorous simulation of 3D masks," *Proc. SPIE on 26th Annual BACUS Symposium on Photomask Technology*, Monterey, Vol. 6349, CA, USA, 2006.
25. Wang, Y. J., W. J. Koh, and C. K. Lee, "Electromagnetic coupling analysis of transient signal through slots or apertures perforated in a shielding metallic enclosure using FDTD methodology," *Progress In Electromagnetics Research*, PIER 36, 247–264, 2002.
26. Bruge, S., "Benchmark of FEM, waveguide and FDTD algorithms for rigorous mask simulation," *Proc. SPIE on 25th Annual BACUS Symposium on Photomask Technology, Monterey*, Vol. 5992, CA, USA, 2005.